

Coherent control based on quantum Zeno and anti-Zeno effects: Role of coherences and timing

Jacob Levitt¹ and Artur F. Izmaylov^{2,3,*}

¹*Cortex Fusion Systems, Inc., New York, NY, 10128, United States*[†]

²*Department of Physical and Environmental Sciences,
University of Toronto Scarborough, Toronto, Ontario, M1C 1A4, Canada*

³*Chemical Physics Theory Group, Department of Chemistry,
University of Toronto, Toronto, Ontario, M5S 3H6, Canada*

(Dated: August 22, 2023)

The quantum-Zeno and anti-Zeno effects (QZE/AZE) are known for a long time, in a quantum system with coupled levels, the measurement of a particular level population can lead to either acceleration (i.e. AZE) or retardation (i.e. QZE) of its population transfer to other levels. Here we consider how one can control the population flow from a coupled quantum state by measurement at a particular time, and what system parameters are responsible for that. We propose a framework for analysis of quantum Zeno dynamics based on time-dependent density matrix perturbation theory. This framework allows us to clearly separate state populations from their coherences and to predict appearance of either QZE or AZE. We illustrate our analysis on two model systems: 1) two coupled levels and 2) a level coupled to a continuum. In both cases dynamics of quantum coherences play a crucial role, and perturbative considerations allow us to predict the effect of projective measurements. In addition, we have extended our consideration to a closely related coherent control scenario, a unitary transformation altering the sign of a state in a coherent superposition describing the system wavefunction.

I. INTRODUCTION

Exploiting various quantum mechanical effects (e.g. quantum coherences and entanglement) comprises a key development in the arrival of quantum technology into modern society¹. One prodigious insight into quantum control is the quantum-Zeno effect (QZE)²⁻⁷, for which the quantum system can be prevented from sampling certain subspaces of its Hilbert space by applying the appropriate series of projective measurements. Extensions of the QZE to include non-demolition measurements⁸ and unitary operators^{9,10}, as well as the complementary, anti-Zeno effect (AZE), in which the quantum system is forced to sample its own Hilbert space in any arbitrary desired fashion^{6,7,11-13}, all fall under the umbrella of the QZE mechanism¹⁴⁻²². The QZE and AZE have demonstrated diverse utility in key technology areas such as quantum sensing^{19,23-25}, chiral spectroscopy²⁶, integrated photonics^{7,27-32}, quantum communication³²⁻⁴², quantum counterfactual communication⁴²⁻⁴⁸, Bell-state analysis⁴⁹, non-demolition measurement⁵⁰⁻⁵², and quantum computing⁵³⁻⁵⁹. They are generally considered paradigmatic for quantum control^{36,53-58,60-67}: one goal of the present work is to deliver a unified framework of the QZE/AZE with the aspiration that this enables its further penetration into quantum science applications.

Even though both QZE and AZE were modelled and exploited for long time, clear criteria on when one or the other occurs in a particular system have not been fully established. Kofman and Kurizki in their seminal work (2000)¹¹ have shown that both effects can occur in a level coupled to a continuum system. A particular dynamical scenario after the measurement is determined by the overlap of the level broadening (due to the coupling with

the continuum) and the continuum spectral density.^{11,68} This generally corresponds to observing QZE(AZE) if the level is energetically within (outside of) the range of the continuum energies. Yet, there are other model systems, some of them we are considering below, where QZE and AZE can be present in the same system and a switch between them is determined by the time of the measurement.

One clarification on terminology needs to be done here, what is meant by the measurement process in the quantum Zeno dynamics literature refers only to decoherence by the device and not the selection of the pointer state. In other words, the measurement is assumed to produce the mixed state $\rho_M = \sum_i |c_i|^2 |i\rangle \langle i|$ from the initial pure state of the evolving quantum system, $\rho = |\psi\rangle \langle \psi| = \sum_{ij} c_i^* c_j |i\rangle \langle j|$ due to interaction with the measuring device. In this case, the measurement can be seen as enforcing unitary dynamics of the system coupled to the device, which is equivalent to the von Neumann measurement.⁶⁹

Considering that QZE and AZE are related to alternation of coherences by the measurement, one can attempt to control the system by applying unitary transformations that only change signs of its coherences instead of destroying them. Saha *et al.* (2011)⁷⁰ applied a perturbative framework to explore the QZE and AZE for scenarios involving both projective (demolition) and unitary (non-demolition) interactions with a quantum system. Population transfer between two weakly coupled states, where the target state is embedded into a continuum, was shown to be somewhat controlled via modification the timing between successive measurements or unitary rotations that change signs of coherences between system states. In Ref. 71, this result was extended to the prob-

lem of nuclear fusion via a model of tunnelling through coulombic (MeV-scale) barriers providing some evidence that unitary control of a bound nuclear wavepacket can accelerate population transfer to the continuum of fusion product channels. Yet, there was no attempt to elucidate what is responsible for appearance of a particular effect, QZE or AZE.

In this work we would like to clarify the role of quantum coherences that appear during the quantum dynamics associated with the population transfer. Clearly, these coherences are involved in control scenario involving QZE, AZE, or their analogues stimulated by unitary transformations that change system state signs in the system superposition wavefunction. To perform this analysis we will employ time-dependent density matrix perturbation theory, where the perturbation is responsible for coupling between the system states.

II. THEORY

A. Two-level model

Let us consider a two-level model given by the Hamiltonian

$$H = \epsilon_0 |0\rangle \langle 0| + \epsilon_1 |1\rangle \langle 1| + V(|1\rangle \langle 0| + |0\rangle \langle 1|), \quad (1)$$

where ϵ_i are level energies, and V is a coupling. The density matrix of the system is $\rho(t) = \sum_{i,j} \rho_{ij}(t) |i\rangle \langle j|$, satisfying the Liouvilian equation $i\partial_t \rho(t) = [H, \rho(t)]$ with the initial condition $\rho(0) = |0\rangle \langle 0|$ and the population of the 0th state, ρ_{00} , as the quantity of interest. All numerical simulations are done with the two-state model with $V = 0.2$ a.u., $\epsilon_{1/0} = \pm 0.2$ a.u. Here and in what follows we will use atomic units.

To see the QZE and AZE from measurements and unitary transformations, it is convenient to consider perturbation theory analysis of $\rho(t)$ dynamics treating $\hat{V} = V(|1\rangle \langle 0| + |0\rangle \langle 1|)$ as the perturbation. In the interaction picture, $\rho_I(t) = e^{iH_0 t} \rho(t) e^{-iH_0 t}$, up to the second order in perturbation, the density is given as

$$\rho_I(t) = \rho(0) + \rho_I^{(1)}(t) + \rho_I^{(2)}(t), \quad (2)$$

$$\rho_I^{(1)}(t) = -i \int_0^t d\tau [V_I(\tau), \rho(0)], \quad (3)$$

$$\rho_I^{(2)}(t) = - \int_0^t d\tau \int_0^\tau d\tau' [V_I(\tau), [V_I(\tau'), \rho(0)]], \quad (4)$$

where $V_I(\tau) = e^{-iH_0 \tau} \hat{V} e^{iH_0 \tau}$. The first order in V_I pro-

cess produces populations $\rho_{ss}^{(1)}(t)$ from coherences $\rho_{s's'}(0)$

$$\rho_{ss}^{(1)}(t) = -i \langle s | \int_0^t d\tau [V_I(\tau), \rho(0)] | s \rangle \quad (5)$$

$$= -i \int_0^t d\tau \langle s | V_I(\tau) | s' \rangle \rho_{s's}(0) - \rho_{ss'}(0) \langle s' | V_I(\tau) | s \rangle \quad (6)$$

$$= 2\text{Im} \left[\rho_{s's}(0) \int_0^t d\tau \langle s | V_I(\tau) | s' \rangle \right] \quad (7)$$

and coherences $\rho_{s's'}^{(1)}(t)$ from populations $\rho_{ss}(0)$

$$\rho_{s's'}^{(1)}(t) = -i \langle s | \int_0^t d\tau [V_I(\tau), \rho(0)] | s' \rangle \quad (8)$$

$$= i[\rho_{ss}(0) - \rho_{s's'}(0)] \int_0^t d\tau \langle s | V_I(\tau) | s' \rangle, \quad (9)$$

the last equality is the consequence of zero diagonal perturbation terms, $\langle s | V_I(\tau) | s \rangle = 0$. In the second order, due to the absence of the diagonal perturbation elements, there is no contribution from coherences to population dynamics, the only contribution originates from populations

$$\rho_{ss}^{(2)}(t) = \langle s | \int_0^t d\tau \int_0^\tau d\tau' [V_I(\tau), [V_I(\tau'), \rho(0)]] | s \rangle \quad (10)$$

$$= \int_0^t d\tau \int_0^\tau d\tau' \rho_{ss}(0) \langle s | V_I(\tau) V_I(\tau') | s \rangle - \langle s | V_I(\tau) | s' \rangle \rho_{s's'}(0) \langle s' | V_I(\tau') | s \rangle \quad (11)$$

$$= [\rho_{ss}(0) - \rho_{s's'}(0)] \times \int_0^t d\tau \int_0^\tau d\tau' \langle s | V_I(\tau) | s' \rangle \langle s' | V_I(\tau') | s \rangle.$$

To follow populations $\rho_{ss}(t)$ we need to consider two paths: 1) two first order steps, population to coherences [Eq. (9)] and coherences to populations [Eq. (7)], and 2) a single second order process, population to population [Eq. (12)]. For small enough times higher order processes can be ignored because no matter how large V is, it is multiplied by time in all equations for final quantities.

The QZE can be explained by noticing that if measurement destroys coherences, $\rho_{s's'} \rightarrow 0$, then the population transfer path 1 is disrupted because Eq. (7) will have zero coherences at the moment after the measurement. This disruption leaves only path 2 that has a quadratic dependence on time, $\rho_{ss}(t) \sim t^2$, which has a zero slope at $t = 0$ and the time after the measurement (see Fig. 1, here we assume that the measurement is instantaneous).

For understanding the AZE, note that coherences can enhance both forward ($\rho_{00} \rightarrow \rho_{11}$) and backward ($\rho_{11} \rightarrow \rho_{00}$) transfers according to Eq. (7). Figure 2 illustrates that during the forward process negative imaginary part of ρ_{10} coherence builds up and facilitates the transfer via path 1. Due to the sum rule $\sum_s \rho_{ss} = 1$, disruption of the backward transfer is enhancing the forward transfer. Therefore, if the coherences are destroyed by

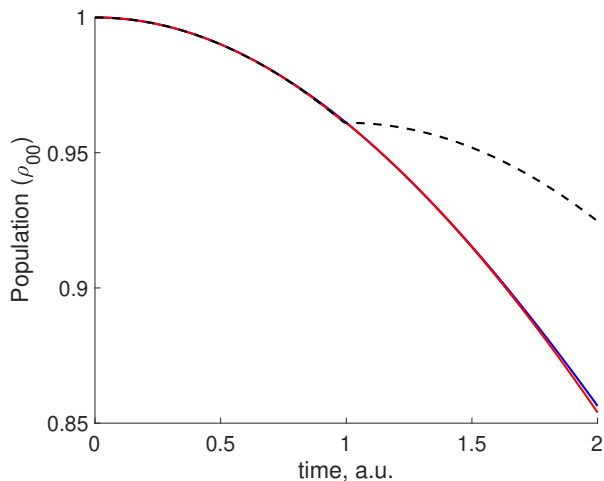


FIG. 1. Population ρ_{00} given by perturbation theory (red solid), exact (blue solid), and exact dynamics with coherences destroyed due to a measurement at 1 a.u. (black dashed).

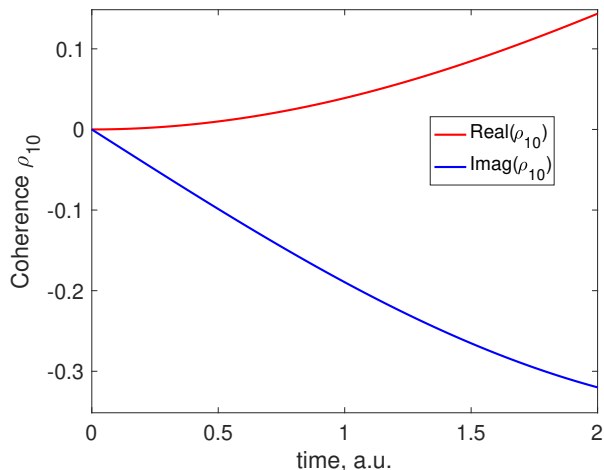


FIG. 2. Coherence ρ_{10} real and imaginary components during the exact dynamics. Negative values of the imaginary part are responsible for positive contribution to the overall population transfer from 0 to 1.

the measurement at the time when their values stimulate backward transfer one will observe the AZE (see Fig. 3). There are few considerations that help understanding these dynamics. First, due to the level energy difference the transfer is incomplete state $|1\rangle$ is only populated 50%, this takes place around 5.5 a.u. This makes population difference $\rho_{00} - \rho_{11}$ always positive and thus path 2 will always favors the forward flow of the population, $\rho_{00} \rightarrow \rho_{11}$. Second, Fig. 4 shows that the imaginary part of coherence ρ_{10} becomes positive after 5.5 a.u., which makes the coherence to facilitate the reverse process, $\rho_{11} \rightarrow \rho_{00}$, according to path 1. Considering these two points, the presence of the AZE on Fig. 3 becomes clear. Destroying the coherences around 5.5 a.u. leaves

only the population channel (path 2) with $\rho_{00} - \rho_{11} \approx 0$ which does not produce either good population transfer or build up of new coherences. If one does the measurement later, 7.5 a.u. or 8.5 a.u., there is a larger population difference $\rho_{00} - \rho_{11}$, but this difference still favours the forward transfer. Also, when the coherence ρ_{10} is destroyed and it starts to build up again, its imaginary part has a different sign than before the measurement (Fig. 4), hence, this also favours the forward path.

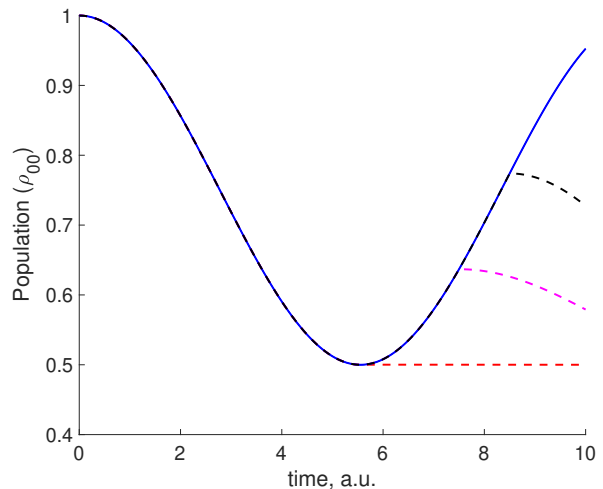


FIG. 3. Population ρ_{00} given by exact dynamics (blue solid) and three measurement induced coherent destruction dynamics that are different in the time of measurement: 5.5 a.u. (black dashed), 7.5 a.u. (magenta dashed), and 8.5 a.u. (blue dashed).

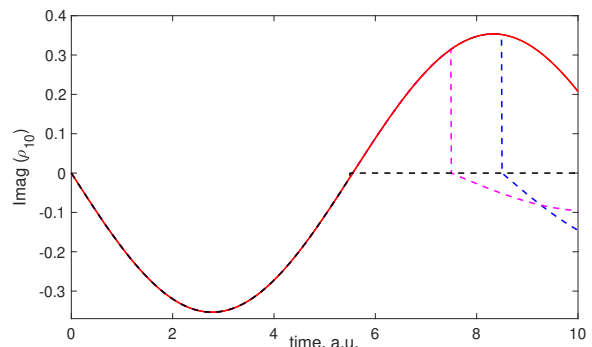


FIG. 4. Imaginary part of ρ_{10} given by exact dynamics (red solid) and three measurement induced coherence destruction dynamics that are different in the time of measurement: 5.5 a.u. (red dashed), 7.5 a.u. (magenta dashed), and 8.5 a.u. (black dashed).

Moreover, one can see from Eq. (7) that the direction in which coherences sway the population flow depend on the sign of their imaginary part. Thus, if one can change only the sign of coherences it will be enough to change the direction of the population flow from Eq. (7). This sign

change can be accomplished by the unitary transformation $U = 1 - 2|0\rangle\langle 0|$, which is also hermitian $U^\dagger = U$. U is changing the sign of the coherences without changing populations

$$U^\dagger \rho U = \rho_{00} |0\rangle\langle 0| + \rho_{11} |1\rangle\langle 1| - \rho_{01} |0\rangle\langle 1| - \rho_{10} |1\rangle\langle 0|. \quad (12)$$

Figure 5 shows how U changes the population transfer if applied in different times. When applied before the imaginary part of the ρ_{10} coherence switches from negative to positive ($t < 5.5$ a.u. according to Fig. 4) the U sign-flipping effect will be similar to the QZE. However, if U is applied when $\text{Im}[\rho_{10}] > 0$, $t > 5.5$ a.u., it enhances the AZE to the point where more forward population transfer becomes possible. Note that because U flips the sign of non-eigenstate coherences, it can change the system energy.

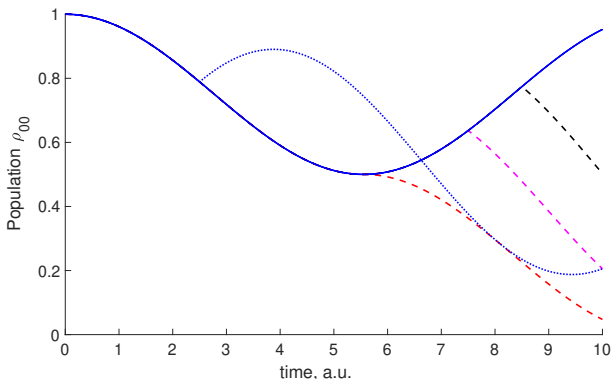


FIG. 5. Population ρ_{00} given by exact dynamics (blue solid) and four U induced coherence sign-flip dynamics that are different in the time of U application: 2.5 a.u. (blue dotted), 5.5 a.u. (black dashed), 7.5 a.u. (magenta dashed), and 8.5 a.u. (blue dashed).

To avoid dependence on limitations of perturbation theory at longer times, we continue here with a parallel non-perturbative consideration, which provides the following equations of motion:

$$i\partial_t \rho_{jj} = \langle j| [H, \rho] |j\rangle = \sum_k H_{jk} \rho_{kj} - \rho_{jk} H_{kj} \quad (13)$$

$$i\partial_t \rho_{jk} = \langle j| [H, \rho] |k\rangle = \sum_l H_{jl} \rho_{lk} - \rho_{jl} H_{lk} \quad (14)$$

$$= \sum_l H_{lj} \rho_{lk} - \rho_{lj}^* H_{lk} \quad (15)$$

$$= (\epsilon_j - \epsilon_k) \rho_{jk} - (\rho_{jj} - \rho_{kk}) V, \quad (16)$$

where we used real character of our Hamiltonian matrix elements $H_{jk} = H_{kj}$ and hermiticity of the density matrix $\rho_{jk} = \rho_{kj}^*$. Considering that dynamics is unitary and populations always stay real gives

$$\partial_t \text{Re}[\rho_{jj}] = \sum_{k \neq j} 2H_{jk} \text{Im}(\rho_{kj}), \quad (17)$$

this shows importance of signs and magnitudes of the imaginary parts of coherences for the population dynamics. For the 2-level system this provides $\partial_t \text{Re}[\rho_{00}] = 2V \text{Im}(\rho_{01})$.

It is also useful to have the expressions for time derivatives of real and imaginary parts of coherences

$$\partial_t \text{Re}(\rho_{jk}) = (\epsilon_j - \epsilon_k) \text{Im}(\rho_{jk}) \quad (18)$$

$$\partial_t \text{Im}(\rho_{jk}) = (\rho_{jj} - \rho_{kk}) V - (\epsilon_j - \epsilon_k) \text{Re}(\rho_{jk}). \quad (19)$$

Since both QZE and AZE heavily depend on coherence dynamics it is worth emphasizing that a significant difference between dynamics of the system after the measurement and after the U transformation is the presence of the $\text{Re}(\rho_{jk})$ term [Eq. (19)]. The measurement destroys coherences and make the $\text{Re}(\rho_{jk})$ term zero, while U only inverts its sign. The implications of this is already visible by comparing Fig. 3 and Fig. 5, the latter has much more pronounced AZE at 5.5 a.u.

B. Level coupled to a continuum

The Hamiltonian for this type of systems is

$$H = \epsilon_0 |0\rangle\langle 0| + \sum_k \epsilon_k |k\rangle\langle k| + V(|k\rangle\langle 0| + |0\rangle\langle k|), \quad (20)$$

where $V = 0.01$, $\epsilon_k \in [-D, D]$, $D = 5$ a.u., $\epsilon_0 = 0$ for the level in a continuum (LIC) model and $\epsilon_0 = D + 0.04$ for the level outside of a continuum (LOC) model. In our simulations, the continuum is modelled by 200 discrete levels uniformly distributed in the $[-D, D]$ range so that $\epsilon_{k+1} - \epsilon_k = 0.05$ a.u.

a. The level in a continuum model: Exact dynamics starting at the $|0\rangle$ state gives the population decay to the continuum (Fig. 6). As expected, there is an exponential decay of the population which has a recurrence at later time due to a finite continuum discretization (the recurrence is not shown on the figure). When at various times we perform measurements collapsing all coherences that are created, the overall trend is the QZE, slowing down the transfer from the $|0\rangle$ state to the continuum. The questions that arise are what explains the QZE here and why it is getting stronger at later time. For both questions, it is instructive to consider a total imaginary part of all coherences between the level and the continuum states, $\Sigma = \sum_k \text{Im}[\rho_{0k}]$ (Fig. 7). According to Eq. (17), Σ is the quantity that determines the coherence channel of the population transfer. Figure (7) reveals a few trends in Σ dynamics. Initially, Σ quickly becomes negative via oscillations that also quickly reduce the amplitude and turn into a stable growth of Σ . This $\Sigma(t)$ dynamics can be easily understood from the perturbation theory point of view for the first order channel from the populations to coherences, Eq. (9). Integrating the time and taking imaginary part in Eq. (9) for our model gives

$$\Sigma^{(1)}(t) = V \sum_k \Delta \rho_k \frac{\sin(\Delta \epsilon_k t)}{\Delta \epsilon_k}, \quad (21)$$

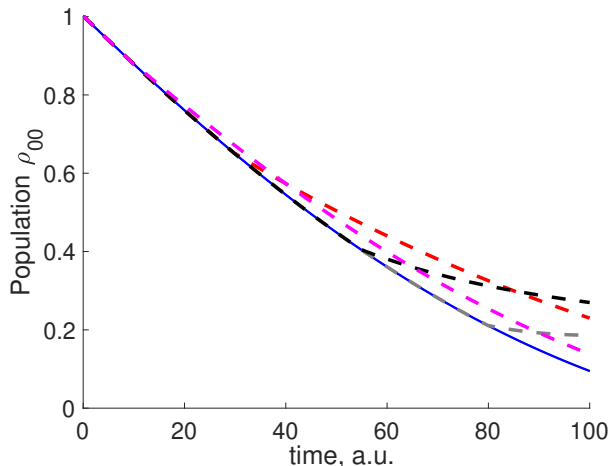


FIG. 6. Population ρ_{00} given by exact dynamics (blue solid) and four measurement induced decoherences that are done in different times: 10 a.u. (magenta dashed), 30 a.u. (red dashed), 55 a.u. (black dashed), and 80 a.u. (grey dashed).

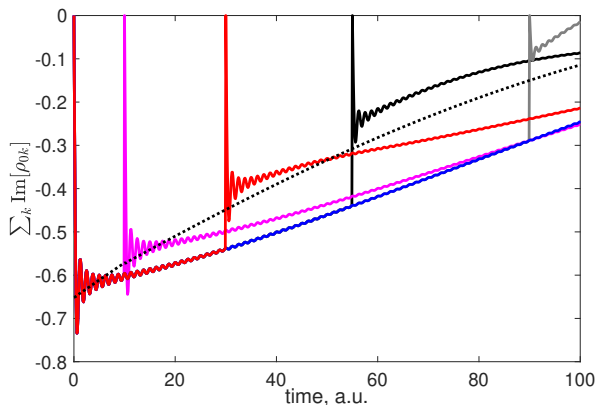


FIG. 7. Sum of imaginary part of coherences between the level and continuum states ($\Sigma(t)$) as a function of time, given by exact dynamics (blue solid) and four measurement induced decoherences that are done in different times: 10 a.u. (magenta dashed), 30 a.u. (red dashed), 55 a.u. (black dashed), and 90 a.u. (grey dashed). The dotted black line is $\Sigma^{(1)}(t_{\min})$ from Eq. (23), its time dependence comes from $\Delta\rho_k$ evaluated along the exact dynamics.

where $\Delta\rho_k = \rho_{kk} - \rho_{00}$ and $\Delta\epsilon_k = \epsilon_k - \epsilon_0$. Clearly, all $\Delta\rho_k$ are -1 at the initial time, and sum of $\sin(\Delta\epsilon_k t)/\Delta\epsilon_k$ stabilizes very quickly due to cancellations of oscillations from different frequencies $\Delta\epsilon_k$. The overall growth of $\Sigma(t) \approx \Sigma^{(1)}(t)$ comes from a time-dependence of $\Delta\rho_k$ that is assumed to be negligible in the first order of perturbation theory.

The negative values of Σ along the dynamics stimulates forward population flow $\rho_{00} \rightarrow \rho_{kk}$ via coherences (Eq. (7) or Eq. (17)). Because of $\Sigma(t)$ growth with time, this channel becomes weaker. To understand the QZE, we only need to notice that after the disruption of the co-

herence channel $\Sigma(t)$ returns to higher values than before the measurement, thus the coherent channel for the population transfer is weakened by the measurement. Figure (7) shows this clearly if we compare the $\Sigma(t)$ level dips right after the measurements and the $\Sigma(t)$ level in dynamics without measurements. Yet, this still leaves a question why $\Sigma(t)$ plunges right after the measurement?

The dip of $\Sigma(t)$ right after the measurement can be well described using the perturbation theory from Eq. (21). Considering that only short time is required to reach the first minimum of $\Sigma(t)$ in t , one can easily find approximations to t_{\min} and $\Sigma(t_{\min})$ using a Taylor decomposition for $\sin(\Delta\epsilon_k t) \approx \Delta\epsilon_k t - \Delta\epsilon_k^3 t^3/6$ in $\Sigma^{(1)}(t)$,

$$t_{\min} = \sqrt{2 \frac{|\sum_k \Delta\rho_k|}{|\sum_k \Delta\rho_k \Delta\epsilon_k^2|}} \quad (22)$$

$$\Sigma^{(1)}(t_{\min}) = -\frac{V}{3} \frac{|2\sum_k \Delta\rho_k|^{3/2}}{|\sum_k \Delta\rho_k \Delta\epsilon_k^2|^{1/2}}. \quad (23)$$

Figure (7) shows that $\Sigma^{(1)}(t_{\min})$ approximates well the first minima right after each measurement in $\Sigma(t)$. Every time the measurement is done, $\Sigma(t)$ vanishes first and then quickly returns to values well approximated by $\Sigma^{(1)}(t_{\min})$ but with different values of $\Delta\rho_k$ that evolve in time (Fig. 7). When we calculate $\Sigma^{(1)}(t_{\min})$ we use time-dependent $\Delta\rho_k$ from exact quantum dynamics. To summarize, the QZE in this case occurs from weakening the coherence channel by zeroing the coherences, this leads to a higher $\Sigma(t)$ level due to higher values of $\Delta\rho_k$ than at the starting point of the dynamics.

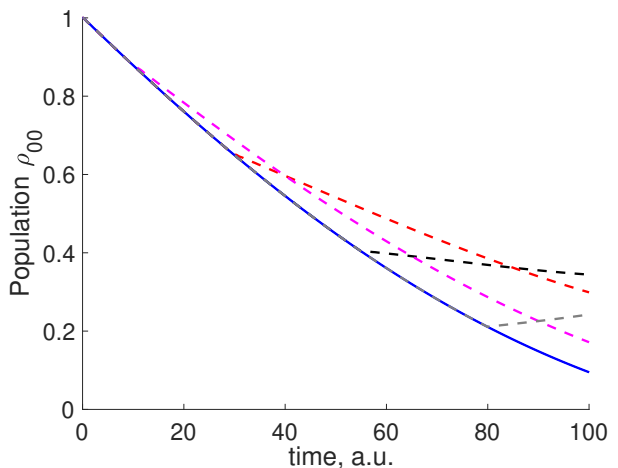


FIG. 8. Population ρ_{00} given by exact dynamics (blue solid) and four U induced coherence sign-flip dynamics that are different in the time of U application: 10 a.u. (magenta dashed), 30 a.u. (red dashed), 55 a.u. (black dashed), and 80 a.u. (grey dashed).

For the experiment with the unitary transformation that changes the signs of all coherences between the level and the continuum, $U = 1 - 2|0\rangle\langle 0|$, trends in population (Fig. 8) and coherence (Fig. 9) dynamics are similar

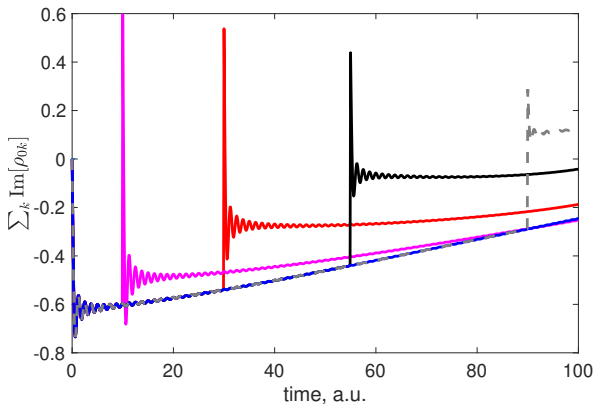


FIG. 9. Sum of imaginary part of coherences between the level and continuum states, given by exact dynamics (blue solid) and four U induced coherence sign-flip dynamics that are different in the time of U application: 10 a.u. (magenta dashed), 30 a.u. (red dashed), 55 a.u. (black dashed), and 90 a.u. (grey dashed).

to those where measurements are used for disrupting the dynamics (Fig. 6 and Fig. 7). The main difference is somewhat stronger QZE that can be connected to higher levels of $\Sigma(t)$ minima right after altering the sign of coherences. This can be attributed to higher initial values of imaginary parts of coherences right after the U action and the second term in Eq. (19), this term was zero when the coherences vanished due to measurements.

b. The level outside of a continuum model: Since $|0\rangle$ level's energy ϵ_0 is further away energetically from energies of levels representing the continuum, in this case the population dynamics oscillates between 1 and 0.83 in ρ_{00} (Fig. 10). When measurements applied along the dynamics they lead to the AZE. What are the reasons for this switch? Considering $\Sigma(t)$ dynamics helps to provide the answer to this question (Fig. 11). The main difference between the LOC and LIC models is that in LOC $\Sigma^{(1)}(t_{\min})$ stays at approximately the same level for all times and this level is below the rise of $\Sigma(t)$ due to natural dynamical decoherence described by long term limit of Eq. (21) (compare blue solid and dotted black lines on Fig. 11). Thus, every time we measure ρ_{00} in LOC, $\Sigma(t)$ very quickly goes to $\approx \Sigma^{(1)}(t_{\min})$, which stimulates the coherence channel of the population transfer. This relation is the opposite to the one we observed in the LIC model, there $\Sigma^{(1)}(t_{\min}) > \Sigma(t)$ (compare blue solid and dotted black lines on Fig. 7).

When coherent control of LOC dynamics is done by U , the trends in population (Fig. 12) and coherence (Fig. 13) dynamics are more intense compared to those when measurements were used: reduction of Σ after the sign flip is lower than after zeroing it with the measurement, so the AZE is even more pronounced. We attribute this to similar factors as in the LIC model, not zeroing the coherences but rather changing their signs changes the initial conditions for dynamics after the U influence and opens

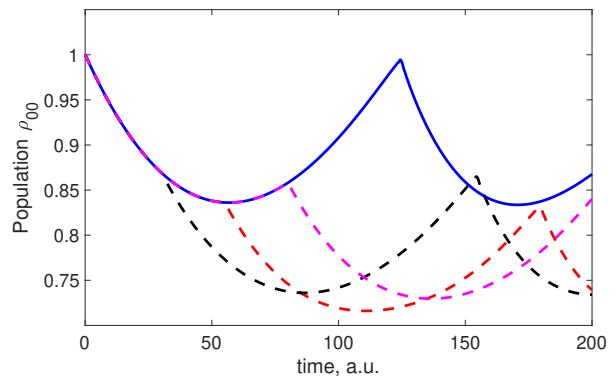


FIG. 10. Population ρ_{00} given by exact dynamics (blue solid) and four measurement induced decoherences that are done in different times: 30 a.u. (black dashed), 55 a.u. (red dashed), and 80 a.u. (magenta dashed).

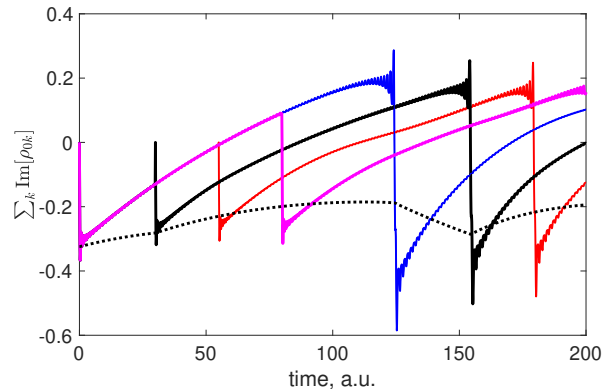


FIG. 11. Sum of imaginary part of coherences between the level and continuum states, given by exact dynamics (blue solid) and four measurement induced decoherences that are done in different times: 30 a.u. (black solid), 55 a.u. (red solid), and 80 a.u. (magenta solid). The dotted black line is $\Sigma^{(1)}(t_{\min})$ from Eq. (23), its time dependence comes from $\Delta\rho_k$ evaluated along the exact dynamics.

another channel for Σ modification (the second term in Eq. (19)).

III. CONCLUSIONS

In this work we have shown on a microscopic level using simple models how the quantum Zeno and anti-Zeno effects operate. For the first time, a simple picture involving density matrix perturbation theory in low orders is used to explain coherent control that leads to these effects. The two scenarios that were considered are either zeroing coherences by doing measurements or altering signs of coherences by performing a unitary transformation. Qualitatively, these two control scenarios gave the same results, the main difference was only quanti-

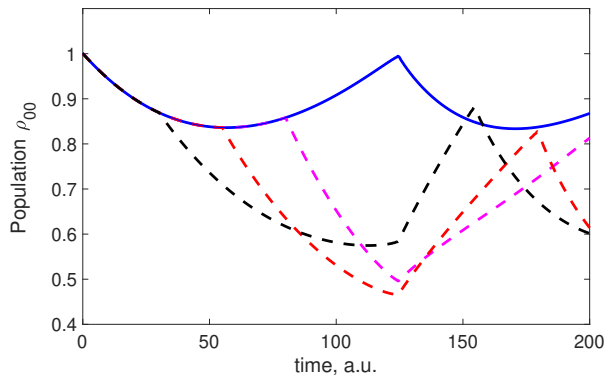


FIG. 12. Population ρ_{00} given by exact dynamics (blue solid) and four U induced coherence sign-flip dynamics that are different in the time of U application: 30 a.u. (black dashed), 55 a.u. (red dashed), and 80 a.u. (magenta dashed).

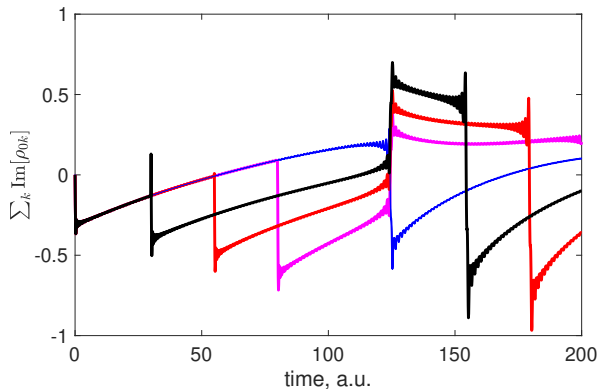


FIG. 13. Sum of imaginary part of coherences between the level and continuum states, given by exact dynamics (blue solid) and four U induced coherence sign-flip dynamics that are different in the time of U application: 30 a.u. (black solid), 55 a.u. (red solid), and 80 a.u. (magenta solid).

tative, the unitary transformation usually intensifies either quantum-Zeno or anti-Zeno effect that can be in-

duced by the measurement decoherence. The situation is more interesting in consideration of whether one would observe the quantum-Zeno or anti-Zeno effect in a particular setup. We have reached the conclusion that using only perturbative considerations and accurate values of state populations are sufficient to determine what effect will be observed. If one needs to predict this for longer time-scales it is safer to take state populations from the exact dynamical simulations.

Both quantum-Zeno and anti-Zeno effects are examples of the coherent control because they originate from changes in quantum coherences that are induced by the measurement or application of the sign-changing unitary transformation. To understand both effects, one simply needs to realize that in the perturbation theory picture there are two channels of the transfer for population of one level to population of other levels: 1) the direct second-order transfer of population to population and 2) the two-step transfer, where each steps are of the first order in perturbation, first, from population to coherence and then from coherence to population. Coherent control processes discussed in this work alter the second channel, when this alternation leads to reduction of the coherence channel capacity this gives rise to the quantum-Zeno effect, otherwise we have the anti-Zeno effect. Interestingly, the same manipulations done at different times or on different systems can lead to the opposite effects. This can be understood simply because coherences between any two states can stimulate both forward and backward transfers, depending on the sign of their imaginary part. Also, in general, coherences undergo their own dynamics, therefore they provide a flexible framework for controlling population transfer processes.

ACKNOWLEDGEMENTS

A.F.I. is grateful to Jeremy Schofield for stimulating conversations and thanks the Natural Sciences and Engineering Research Council of Canada for financial support.

* artur.izmaylov@utoronto.ca

† jakelevitt@cortexfusion.systems

¹ G. J. Milburn, *Schrödinger's Machines: Machines: The Quantum Technology Reshaping Everyday Life* (W.H. Freeman, New York, NY, 1997).

² B. Misra and E. G. Sudarshan, *Journal of Mathematical Physics* **18**, 756 (1977).

³ W. M. Itano, D. J. Heinzen, J. J. Bollinger, and D. J. Wineland, *Physical Review A* **41**, 2295 (1990).

⁴ A. Kofman and G. Kurizki, *Physical Review A* **54**, R3750 (1996).

⁵ D. Home and M. Whitaker, *Annals of Physics* **258**, 237 (1997).

⁶ K. Koshino and A. Shimizu, *Physics reports* **412**, 191 (2005).

⁷ K. Thapliyal, A. Pathak, and J. Peřina, *Physical Review A* **93**, 022107 (2016).

⁸ M. Gagen and G. Milburn, *Physical Review A* **45**, 5228 (1992).

⁹ P. Facchi, D. Lidar, and S. Pascazio, *Physical Review A* **69**, 032314 (2004).

¹⁰ D. Dhar, L. K. Grover, and S. M. Roy, arXiv preprint quant-ph/0504070 (2005).

¹¹ A. Kofman and G. Kurizki, *Nature* **405**, 546 (2000).

¹² P. Facchi, H. Nakazato, and S. Pascazio, *Physical Review Letters* **86**, 2699 (2001).

- ¹³ M. Yamaguchi, T. Asano, and S. Noda, *Optics Express* **16**, 18067 (2008).
- ¹⁴ M. C. Fischer, B. Gutiérrez-Medina, and M. G. Raizen, *Physical review letters* **87**, 040402 (2001).
- ¹⁵ P. Facchi and S. Pascazio, *Physical review letters* **89**, 080401 (2002).
- ¹⁶ F. Schäfer, I. Herrera, S. Cherukattil, C. Lovecchio, F. S. Cataliotti, F. Caruso, and A. Smerzi, *Nature communications* **5**, 3194 (2014).
- ¹⁷ A. Signoles, A. Facon, D. Grosso, I. Dotsenko, S. Haroche, J.-M. Raimond, M. Brune, and S. Gleyzes, *Nature Physics* **10**, 715 (2014).
- ¹⁸ S. Gherardini, S. Gupta, F. S. Cataliotti, A. Smerzi, F. Caruso, and S. Ruffo, *New Journal of Physics* **18**, 013048 (2016).
- ¹⁹ M. M. Müller, S. Gherardini, and F. Caruso, *Scientific reports* **6**, 1 (2016).
- ²⁰ P. Facchi and S. Pascazio, *Journal of Physics A: Mathematical and Theoretical* **41**, 493001 (2008).
- ²¹ P. G. Kwiat, A. G. White, J. R. Mitchell, O. Nairz, G. Weihs, H. Weinfurter, and A. Zeilinger, *Physical Review Letters* **83**, 4725 (1999).
- ²² H. Zheng, S. Y. Zhu, and M. S. Zubairy, *Physical Review Letters* **101** (2008), 10.1103/physrevlett.101.200404.
- ²³ S. Virzì, A. Avella, F. Piacentini, M. Gramegna, T. Opatrny, A. G. Kofman, G. Kurizki, S. Gherardini, F. Caruso, I. P. Degiovanni, *et al.*, *Physical Review Letters* **129**, 030401 (2022).
- ²⁴ H.-V. Do, C. Lovecchio, I. Mastroserio, N. Fabbri, F. S. Cataliotti, S. Gherardini, M. M. Müller, N. Dalla Pozza, and F. Caruso, *New Journal of Physics* **21**, 113056 (2019).
- ²⁵ X. Long, W.-T. He, N.-N. Zhang, K. Tang, Z. Lin, H. Liu, X. Nie, G. Feng, J. Li, T. Xin, *et al.*, *Physical Review Letters* **129**, 070502 (2022).
- ²⁶ J.-L. Wu, Y. Wang, S.-L. Su, Y. Xia, Y. Jiang, and J. Song, *Optics Express* **28**, 33475 (2020).
- ²⁷ Q. Liu, W. Liu, K. Ziegler, and F. Chen, *Physical Review Letters* **130**, 103801 (2023).
- ²⁸ S. Longhi, *Physical review letters* **97**, 110402 (2006).
- ²⁹ M. Das, K. Thapliyal, B. Sen, J. Peřina, and A. Pathak, *Physical Review A* **103**, 013713 (2021).
- ³⁰ M. Das, B. Sen, K. Thapliyal, and A. Pathak, *arXiv preprint arXiv:2304.04073* (2023).
- ³¹ D. Zezyulin, V. Konotop, G. Barontini, and H. Ott, *Physical review letters* **109**, 020405 (2012).
- ³² Y.-P. Huang, J. B. Altepeter, and P. Kumar, *Physical Review A* **82**, 063826 (2010).
- ³³ I. Nodurft, B. Kirby, R. Glasser, H. Shaw, and T. Searles, in *Quantum 2.0* (Optica Publishing Group, 2022) pp. QTu2A-5.
- ³⁴ I. C. Nodurft, H. C. Shaw, R. T. Glasser, B. T. Kirby, and T. A. Searles, *Optics Express* **30**, 31971 (2022).
- ³⁵ B. C. Jacobs and J. Franson, *Physical Review A* **79**, 063830 (2009).
- ³⁶ L. Zhou, S. Yang, Y.-x. Liu, C. Sun, F. Nori, *et al.*, *Physical Review A* **80**, 062109 (2009).
- ³⁷ S. Hendrickson, C. Weiler, R. Camacho, P. Rakich, A. Young, M. Shaw, T. Pittman, J. Franson, and B. Jacobs, *Physical Review A* **87**, 023808 (2013).
- ³⁸ I. Nodurft, B. Kirby, R. Glasser, H. Shaw, and T. Searles, in *APS Division of Atomic, Molecular and Optical Physics Meeting Abstracts*, Vol. 2022 (2022) pp. H06-009.
- ³⁹ N. ten Brinke, A. Osterloh, and R. Schützhold, *Physical Review A* **84**, 022317 (2011).
- ⁴⁰ V. Bayrakci and F. Ozaydin, *Scientific Reports* **12**, 15302 (2022).
- ⁴¹ A. Tavakoli, H. Anwer, A. Hameedi, and M. Bourennane, *Physical Review A* **92**, 012303 (2015).
- ⁴² Y. Cao, Y.-H. Li, Z. Cao, J. Yin, Y.-A. Chen, H.-L. Yin, T.-Y. Chen, X. Ma, C.-Z. Peng, and J.-W. Pan, *Proceedings of the National Academy of Sciences* **114**, 4920 (2017).
- ⁴³ H. Salih, W. McCutcheon, J. R. Hance, and J. Rarity, *npj Quantum Information* **8**, 60 (2022).
- ⁴⁴ H. Salih, Z.-H. Li, M. Al-Amri, and M. S. Zubairy, *Physical review letters* **110**, 170502 (2013).
- ⁴⁵ L. Vaidman, *Physical Review A* **99**, 052127 (2019).
- ⁴⁶ Y. Cao, Y.-H. Li, Z. Cao, J. Yin, Y.-A. Chen, X. Ma, C.-Z. Peng, and J.-W. Pan, in *CLEO: QELS-Fundamental Science* (Optica Publishing Group, 2014) pp. FM4A-6.
- ⁴⁷ I. Alonso Calafell, T. Strömberg, D. Arvidsson-Shukur, L. Rozema, V. Saggio, C. Greganti, N. Harris, M. Prabhu, J. Carolan, M. Hochberg, *et al.*, *npj Quantum Information* **5**, 61 (2019).
- ⁴⁸ Z.-H. Li, M. Al-Amri, and M. S. Zubairy, *Physical Review A* **92**, 052315 (2015).
- ⁴⁹ F. Zaman, Y. Jeong, and H. Shin, *Scientific reports* **8**, 14641 (2018).
- ⁵⁰ X.-s. Ma, X. Guo, C. Schuck, K. Y. Fong, L. Jiang, and H. X. Tang, *Physical Review A* **90**, 042109 (2014).
- ⁵¹ N. Leppenen, L. Lanco, and D. Smirnov, *Physical Review B* **103**, 045413 (2021).
- ⁵² F. Helmer, M. Mariantoni, E. Solano, and F. Marquardt, *arXiv preprint arXiv:0712.1908* (2007).
- ⁵³ S. Maniscalco, F. Francica, R. L. Zaffino, N. L. Gullo, and F. Plastina, *Physical review letters* **100**, 090503 (2008).
- ⁵⁴ S. Hacohe-Gourgy, L. García-Pintos, L. Martin, J. Dressel, and I. Siddiqi, *Physical Review Letters* **120** (2018), 10.1103/physrevlett.120.020505.
- ⁵⁵ G. A. Paz-Silva, A. T. Rezakhani, J. M. Dominy, and D. A. Lidar, *Physical Review Letters* **108** (2012), 10.1103/physrevlett.108.080501.
- ⁵⁶ X.-B. Wang, J. Q. You, and F. Nori, *Physical Review A* **77** (2008), 10.1103/physreva.77.062339.
- ⁵⁷ A. G. Kofman and G. Kurizki, *Physical Review Letters* **93** (2004), 10.1103/physrevlett.93.130406.
- ⁵⁸ P. Harrington, J. Monroe, and K. Murch, *Physical Review Letters* **118** (2017), 10.1103/physrevlett.118.240401.
- ⁵⁹ J. D. Franson, B. C. Jacobs, and T. B. Pittman, *Physical Review A* **70**, 062302 (2004).
- ⁶⁰ M. M. Müller, S. Gherardini, and F. Caruso, *Annalen der Physik* **529**, 1600206 (2017).
- ⁶¹ A. G. Kofman and G. Kurizki, *Physical Review Letters* **87** (2001), 10.1103/physrevlett.87.270405.
- ⁶² A. Pechen, N. Il'in, F. Shuang, and H. Rabitz, *Physical Review A* **74** (2006), 10.1103/physreva.74.052102.
- ⁶³ J. J. W. H. Sørensen, M. Dalggaard, A. H. Kiilerich, K. Mølmer, and J. F. Sherson, *Physical Review A* **98** (2018), 10.1103/physreva.98.062317.
- ⁶⁴ F. Piacentini, A. Avella, E. Rebufello, R. Lussana, F. Villa, A. Tosi, M. Gramegna, G. Brida, E. Cohen, L. Vaidman, I. P. Degiovanni, and M. Genovese, *Nature Physics* **13**, 1191 (2017).
- ⁶⁵ G. Barontini, L. Hohmann, F. Haas, J. Estève, and J. Reichel, *Science* **349**, 1317 (2015).
- ⁶⁶ A. G. Kofman, G. Kurizki, and T. Opatrny, *Physical Review A* **63** (2001), 10.1103/physreva.63.042108.
- ⁶⁷ J. Clausen, G. Bensky, and G. Kurizki, *Physical Review Letters* **104** (2010), 10.1103/physrevlett.104.040401.

- ⁶⁸ J.-M. Zhang, J. Jing, L.-G. Wang, and S.-Y. Zhu, *Phys. Rev. A* **98**, 012135 (2018).
- ⁶⁹ J. von Neumann, *Mathematical Foundations of Quantum Mechanics* (Princeton University Press, Princeton, 1955).
- ⁷⁰ R. Saha and V. S. Batista, *The Journal of Physical Chemistry B* **115**, 5234 (2011).
- ⁷¹ R. Saha, A. Markmann, and V. S. Batista, *Molecular Physics* **110**, 995 (2012).